

# Thick films coating a plate withdrawn from a bath

J.H. Snoeijer<sup>1</sup>, J. Ziegler<sup>1</sup>, B. Andreotti<sup>2</sup>, M. Fermigier<sup>2</sup>, J. Eggers<sup>1</sup>

*School of Mathematics, University of Bristol, University Walk, Bristol BS8 1TW, UK<sup>1</sup>  
PMMH, UMR 7636 CNRS-ESPCI-P6-P7, 10 rue Vauquelin, 75231 Paris Cedex 05, France<sup>2</sup>*

(Dated: October 24, 2018)

We consider the deposition of a film of viscous liquid on a flat plate being withdrawn from a bath, experimentally and theoretically. For any plate speed  $U$ , there is a range of “thick” film solutions whose thickness scales like  $U^{1/2}$  for small  $U$ . These solutions are realized for a partially wetting liquid, while for a perfectly wetting liquid the classical Landau-Levich-Derjaguin (LLD) film is observed, whose thickness scales like  $U^{2/3}$ . The thick film is distinguished from the LLD film by a dip in its spatial profile at the transition to the bath. We calculate the phase diagram for the existence of stationary film solutions as well as the film profiles, and find excellent agreement with experiment.

When a solid object is pulled out of a liquid reservoir, a thin layer of liquid is entrained by viscous drag (Fig. 1). This principle is used widely in coating technology, where it is known as dip coating, because it is one of the simplest ways to deposit a thin film of liquid on a substrate [1]. According to the pioneering work of Landau & Levich [2] and Derjaguin [3] (LLD), a film of unique thickness  $h_{LLD}$  is selected by the speed of withdrawal  $U$ . The LLD solution has remained the basis of coating theory for more than 60 years, having been generalized to include the effects of inertia [4, 5], deposition on curved substrates [6], and non-Newtonian fluids [7]. The relative size of viscous drag and capillary retention in the film is measured by the capillary number  $Ca = U\eta/\gamma$ , where  $\eta$  is the viscosity and  $\gamma$  the surface tension. At the foot of the film, LLD introduced the requirement that the film be matched smoothly to a static capillary meniscus (see Fig. 1), whose size is controlled by the capillary length  $\ell_c = \sqrt{\gamma/\rho g}$ . In the limit of small  $Ca$ , this matching yields  $h_{LLD} = 0.946\ell_c Ca^{2/3}$ , which gives the small- $Ca$  behavior of the LLD line in the phase diagram, cf. Fig. 2.

In this Letter, we show that at a given speed there exists another, thicker film in addition to the LLD film (cf. Figs. 1 and 2). These new solutions *do not* match smoothly to the bath, but exhibit a bump at the foot of the film (cf. Fig. 1 (c)). As we will explain in more detail below, experimentally the thick solutions are most easily produced for partially wetting fluids just above the critical plate speed  $Ca_f$  at which a film begins to be deposited [8]. Our theoretical analysis however is for the long-time limit only, in which the plate is covered completely by a film, so any solution is characterized by a pair  $(h_f, Ca)$ , as shown in Fig. 2.

A striking feature of the new solutions is that they cover a continuous range of thickness  $h_f$  (Fig. 2, grey area). Each of these solutions entrain a different amount of liquid flux  $q$ , representing the volume of liquid withdrawn from the bath per unit time and unit plate length. Clearly, this flux is limited by the flow through the narrow dimple. Below we compute the maximum possible flux through the dimple and show how this provides a

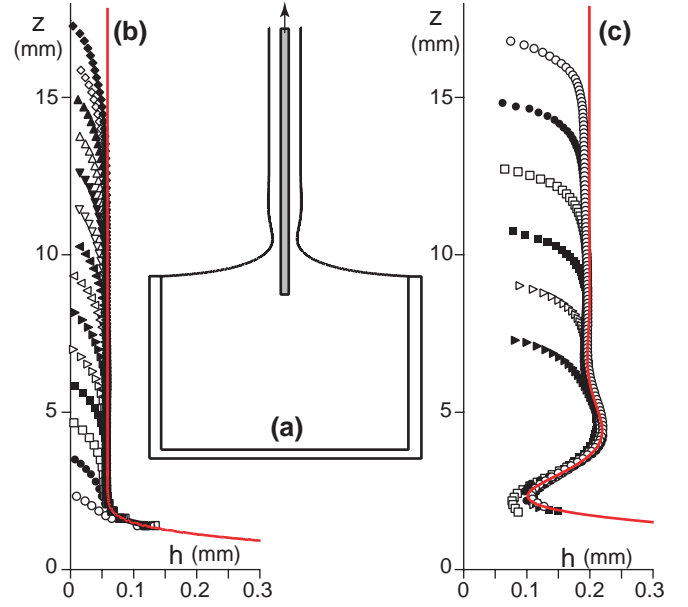


FIG. 1: Fluid films being deposited on a plate withdrawn from a bath of viscous liquid; symbols are experimental measurements of the film profile at successive times. (a) Schematic of the experiment. (b) The fluid wets the plate and deposits a LLD film,  $Ca = 9.27 \times 10^{-3}$ ; the solid line is the classical LLD solution, which predicts  $h_f = 57\mu m$ . (c) The plate is treated such that the fluid wets partially, and deposits a thick film,  $Ca = 8.05 \times 10^{-3}$ ; the solid line is the result of our theory with the film thickness fitted to the experimental result of  $h_f = 198\mu m$ .

lower bound on  $h_f$  (Fig. 2). For larger  $h_f$ , draining due to gravity becomes increasingly important, so at the upper bound (Fig. 2, dashed line) the flux vanishes. Above the dashed line, no solutions are possible, unless the film is alimented from above.

In our theoretical analysis we rescale all lengths by the capillary length  $\ell_c$ . The interface profile is analyzed using the lubrication equation [9] for free surface flows [10]:

$$\kappa' - 1 + \frac{3}{h^2} \left( Ca - \frac{q}{h} \right) = 0. \quad (1)$$

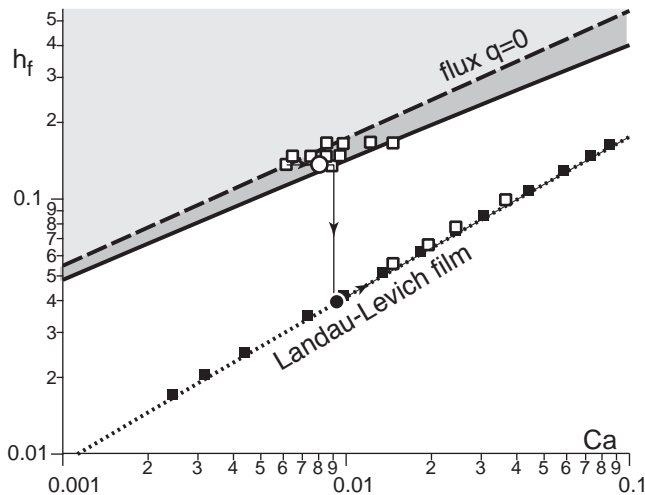


FIG. 2: Phase diagram of stationary solutions in the parameter space  $(h_f, Ca)$ . The dimple solutions exist in the light grey region, but only those in the dark region actually entrain liquid from the bath. The dotted line shows the Landau-Levich solution. The open symbols are for a partial wetting situation, the full symbols for complete wetting; error bars are below the size of the symbols. The two round symbols correspond to the two measurements shown in Fig. 1. The arrows show the experimental path as the speed is slowly increased starting from the dashed line.

Here  $h(z)$  is the interface thickness,  $\kappa$  the interface curvature and  $q$  the flow rate. The three terms correspond to the capillary pressure, gravity, and viscous effects, respectively. For steady solutions, considered here,  $q$  is constant along the plate. Film solutions become asymptotically flat, ( $\kappa = 0$ ), so that the flux can be related to the film thickness  $h_f$  as

$$q = h_f \left( Ca - \frac{h_f^2}{3} \right). \quad (2)$$

Crucially,  $q$  exhibits a non-monotonic dependence on  $h_f$ , owing to gravitational draining (Fig. 3b). For small  $h_f$  the fluid velocity is uniform across the layer and equals the plate velocity, yielding a (dimensionless) flux  $h_f Ca$ . For larger thickness gravity induces draining inside the film, which can even reverse the direction of liquid transport:  $q < 0$  corresponds to transport from the film into the reservoir. As a consequence, the same flow rate  $q$  can be supported by two very different thicknesses of the film. This is why, physically, the thin 'dimple' region can be matched to the much thicker film (Fig. 3).

The interface structure in the dimple region results from a balance between viscosity and surface tension. To describe the profile near the dimple position  $z_d$ , we therefore look for a similarity solution of (1)

$$h = Ca^{2/3} H(\eta), \quad \eta = (z - z_d)/Ca^{1/3}. \quad (3)$$

Following LLD, this solution has the additional property

that the curvature  $h''$  remains finite in the limit of small  $Ca$ , which we are analyzing. This ensures that (3) can be matched to the capillary meniscus of the bath, which has a constant curvature of  $\sqrt{2}$  [11], so the boundary condition in the limit  $\eta \rightarrow -\infty$  is  $H''_{-\infty} = \sqrt{2}$ . Defining  $Q = qCa^{-5/3}$ , one obtains the equation for the dimple

$$H''' + \frac{3}{H^2} \left( 1 - \frac{Q}{H} \right) = 0. \quad (4)$$

So far (4) is the same as for the LLD solution, but the boundary condition toward the flat film region will be less restrictive, so we are able to produce additional solutions. In that region, the curvature becomes small, giving the condition  $H''_{\infty} = 0$ . Below we will justify this argument in more detail.

Figure 4 shows that there is a one-parameter family of solutions  $H(\eta)$ , each corresponding to a different value of  $Q$ , and forming a dimple that matches the thick film to the static bath. The case  $Q = 0$  can be solved analytically [12], while the others have been obtained numerically. We identified a maximum value  $Q_{\max} \approx 1.376$ , above which the boundary conditions can no longer be satisfied. Note that the LLD film is a particular solution of (4), for which  $H$  approaches a constant value rather than shooting back upwards (dotted line).

The final step is to relate the flux through the dimple to the film thickness  $h_f$  at a large distance from the reservoir. Just before  $q(h_f)$  changes sign, it becomes small enough to match the flux in the dimple (cf. Fig. 3). For a small enough capillary number, (2) can be solved to give

$$h_f \simeq (3Ca)^{1/2} - \frac{1}{2} Q Ca^{2/3}, \quad (5)$$

where  $Q \in [0, Q_{\max}]$ . The dimple with  $Q_{\max}$  corresponds to the lowest possible thickness (lower bound of grey region in Fig. 2), while the case  $Q = 0$  marks the upper boundary for  $h_f$  with nonnegative flux. It is worth noting that  $Q = 0$  is only the upper bound in the case of the dip-coating geometry. If an injection of liquid is added at the top of the plate, one could match much thicker films to the bath. The structure of the films will become rather different when the downward flow is much larger than the plate velocity, for which the analysis crosses over to flow down a wall at rest [13].

The similarity solution of (1) corresponding to the film region just above the dimple is

$$h = Ca^{1/2} \tilde{H} \left( \frac{z - z_d}{Ca^{1/6}} \right). \quad (6)$$

In (6), the  $h$ -scale  $Ca^{1/2}$  is dictated by the film thickness (5) for small  $Ca$ . Thus the typical curvature  $h'' \propto Ca^{1/6}$  vanishes in the limit  $Ca \ll 1$ , which establishes the boundary condition  $H''_{\infty} = 0$  quoted above. The slopes in

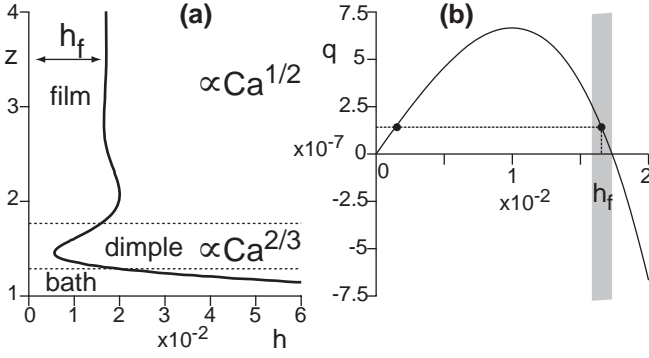


FIG. 3: (a) The three asymptotic regions of the dimple solutions, and the scaling of the respective film thickness with  $Ca$ . (b) The flux  $q$  as function of  $h_f$  at a fixed  $Ca = 10^{-4}$ , cf. (2). The shaded region shows the range of thick solutions at that value of  $Ca$ . The horizontal line illustrates that the flux through the thick film is the same as through the thin dimple region.

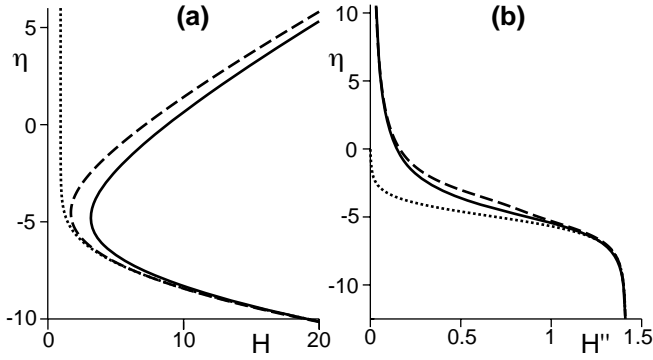


FIG. 4: Various solutions of (4): (a) Dimple profiles with  $Q = 0$  (solid),  $Q_{\max} = 1.376 \dots$  (dashed), and the Landau-Levich film solution for which  $Q \approx 0.946$  (dotted). (b) All curves have  $H''_{\infty} = \sqrt{2}$  to match the curvature of the reservoir, and  $H''_{\infty} = 0$  to match to the film.

the dimple and film regions, as given by (3) and (6), respectively, both scale as  $Ca^{1/3}$  and can thus be matched. To establish our central result (5), a more detailed analysis of the film solutions (6) is not necessary.

Note that the final approach onto the flat film involves (stationary) capillary waves on the film surface that are exponentially damped (see Fig. 3 (a)). From the point of view of the lubrication equation (1), these waves provide an additional degree of freedom that is necessary to achieve different values of flux [4, 14, 15]. Linearizing around the flat film, one finds that such waves can in principle exist when  $h_f > Ca^{1/2}$ . As can be seen from (5), however, this condition is not sufficient to explain the new films. Similar dimpled solutions have also been found for Marangoni-driven flows [16].

*Experimental methods* – In our experiment, a silicon wafer is withdrawn vertically from a bath of silicone oil (viscosity  $\eta = 4.95 \text{ Pa}\cdot\text{s}$ , surface tension  $\gamma =$

$0.0203 \text{ N}\cdot\text{m}^{-1}$ , density  $\rho = 970 \text{ kg}\cdot\text{m}^{-3}$ , molecular size  $70 \text{ nm}$ ) by a step-motor. The silicon wafer is totally wetted by the silicone oil. When coated with the fluorinated surfactant FC725, partial wetting conditions are obtained. Depending on the protocol, the contact angle lies between  $48^\circ$  and  $55^\circ$ , with an hysteresis of  $5^\circ$ . The film thickness  $h_f$  is measured by spectrometry. A reflection probe made of a tight bundle of six illumination fibers around one read fiber is placed at  $5 \text{ mm}$  from the plate. It is connected to a Tungsten Halogen light source and to a diffraction-grating spectrometer resolving visible and near-infrared wavelengths. The relative resolution, limited by the entrance slit and the size of the photo-sensitive elements, is around  $0.25 \text{ nm}$ . A 3648-element linear CCD-array detector measures the intensity as a function of the wavelength  $\lambda$ , averaged over  $4s$ . Defects of the CCD are calibrated in the absence of film and corrected to improve the signal-to-noise ratio. Once a film is present, the spectrum contains oscillations of the form  $\cos(4\pi n h_f / \lambda)$ , where  $n = 1.4034$  is the refractive index of silicone oil. By fitting the spectrum, the thickness  $h_f$  can be measured to within  $0.2\%$  up to a thickness of  $240 \mu\text{m}$  (cf. Fig. 5).

The spatial profile of the entrained film is measured by placing a  $200 \mu\text{m}$  wire at a distance  $d = 14 \pm 1 \text{ mm}$  from the silicon wafer. The mirror image of the wire (reflected in the silicon plate) is distorted by refraction through the liquid/vapor interface of local slope  $h'$ , making the system equivalent to a wire placed at a distance  $d$  behind a prism of (small) angle  $2h'$ . At small angles, the rays are thus deflected by an angle  $2(n-1)h'$  in the direction of steepest slope, independent of the incident angle. Hence the mirror image of the wire is vertically displaced by a distance  $2(n-1)dh'$ . The wire is imaged with a  $2048 \times 2048$  CCD camera, fitted with a  $60 \text{ mm}$  macro lens. The position of the wire image is determined by image inter-correlation, achieving sub-pixel resolution.

We have calibrated the relation between the displacement and the local interface slope by two independent methods. First, we have replaced the oil film by optical glass prisms ( $n = 1.52$ ) of angle  $1^\circ$ ,  $2^\circ$ ,  $3^\circ$  and  $4^\circ$ . We obtain a resolution of  $950 \pm 30$  pixels per unit slope ( $16.5 \text{ pixels/o}$ ), once the index difference between oil and glass is taken into account. Second, using the step-motor, we have determined an image resolution of  $11.7 \mu\text{m/pixels}$ , which leads to  $970 \pm 70$  pixels per unit slope. To summarize, the displacement of the image of the wire gives the local interface slope from which we reconstruct the film profile, by integration. The constant of integration is fixed in the flat region of the film, using the value of  $h_f$  measured by spectrometry. There are two sources of error in the final reconstruction: an absolute uncertainty of  $3\%$  in the slope, and the error from the spatial integration of the random noise present for each point.

Finally, we return to the question of how a particular

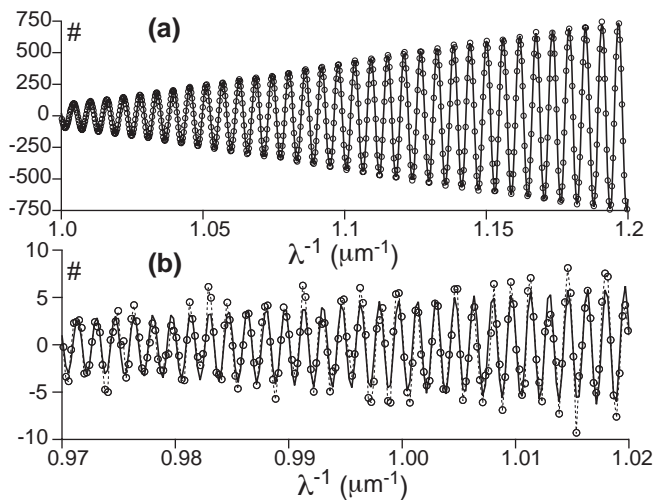


FIG. 5: Measurement of the film thickness by spectroscopy. The free charge carriers produced by photon absorption are accumulated during 0.4 s, counted and displayed as a function of the inverse wavelength  $\lambda^{-1}$ . This spectrum is averaged over 100 realizations and corrected from the effect of CCD heterogeneities, calibrated previously. It is then split into the sum of a smooth spectrum, characteristic of the light source, and an oscillating spectrum, shown above (symbols). It is finally fitted by a sine modulated in amplitude by a Gaussian envelope (solid line). (a) LLD film at  $Ca = 9.75 \times 10^{-2}$ . The best fit gives  $h_f = 61.24$  nm with (formally) a statistical accuracy of 0.005 nm. However, the reproducibility of two complete experimental runs is only to within 0.1 nm. (b) Thick film at  $Ca = 8.53 \times 10^{-2}$ . The best fit gives  $h_f = 214.68$  nm with (formally) a statistical accuracy of 0.05 nm and a reproducibility to within 1 nm. Thick films are at the limit of resolution, hence the interference pattern is only visible in the near-infrared range of wavelengths.

type of film solution is realized experimentally. As shown in [8], the front of a liquid film of partially wetting fluid possesses a characteristic speed of recession  $Ca_f$  relative to the substrate, which is essentially set by the contact angle. Since the flux  $q$  through the contact line is zero, according to (2) this translates into a characteristic film thickness  $h_f = (3Ca_f)^{1/2}$ . Thus if the plate speed  $Ca$  is marginally above  $Ca_f$ , the contact line moves up the plate very slowly, and the flux through the liquid film is close to zero: one has prepared the state  $(h_f, h_f^2/3)$  at the upper end of the thick film solutions.

If the plate speed is now slowly increased, as we did in an experimental run shown in Fig. 2 by the arrows, one moves horizontally into the grey region, since  $h_f$  is fixed by the motion of the contact line. As the end of the grey region is reached, the solution falls off the region of allowed solutions, and a LLD solution is realized instead (cf. Fig. 2). During this transition, the dimple detaches

from the bath, and moves up the plate, leaving behind the LLD film. In effect, this is the situation described in our earlier paper [8]. Note that we were not able to take a measurement right above the transition, since the LLD film takes too long to develop. Of course the above does not imply that thick films can only be produced in partial wetting situations. The most promising experimental setup to produce a thick film is that of viscous flow in the interior of a cylinder, which can be rotated in both senses. This offers considerably more flexibility in preparing thicker films.

In conclusion, we have calculated a phase diagram for film coating from a bath. At a given speed, two different types of film solutions are possible. The novel, thick films described here are easily realized experimentally, and experiment agrees extremely well with theoretical prediction.

We gratefully acknowledge Howard Stone and Wiebke Drenckhan for clarifying discussions and Giles Delon for sharing his experimental expertise. J.H.S. acknowledges support from a Marie Curie European Action FP6 (Grant No. MEIF-CT-2006-025104).

- 
- [1] S. J. Weinstein and K. J. Ruschak, *Annu. Rev. Fluid Mech.* **36**, 29 (2004).
  - [2] L. D. Landau and B. V. Levich, *Acta physico-chimica USSR* **17**, 42 (1942).
  - [3] B. V. Deryaguin, *Acta physico-chimica USSR* **20**, 349 (1943).
  - [4] B. Jin, A. Acrivos, and A. Munch, *Phys. Fluids* **17**, 103603 (2005).
  - [5] A. de Ryck and D. Quéré, *J. Colloid Interf. Sci.* **203**, 278 (1998).
  - [6] D. Quéré, *Annu. Rev. Fluid Mech.* **31**, 347 (1999).
  - [7] A. de Ryck and D. Quéré, *Langmuir* **14**, 1911 (1998).
  - [8] J. H. Snoeijer, G. Delon, B. Andreotti, and M. Fermigier, *Phys. Rev. Lett.* **96**, 174504 (2006).
  - [9] At small  $Ca$  viscous effects become negligible whenever  $h' \gtrsim 1$ , so that the equation remains valid in the bath.
  - [10] A. Öron, S. H. Davis, and S. G. Bankoff, *Rev. Mod. Phys.* **69**, 931 (1997).
  - [11] L. D. Landau and E. M. Lifshitz, *Fluid Mechanics* (Pergamon: Oxford, 1984).
  - [12] B. R. Duffy and S. K. Wilson, *Appl. Math. Lett.* **63**, 63 (1997).
  - [13] S. D. R. Wilson and A. F. Jones, *J. Fluid Mech.* **128**, 219 (1983).
  - [14] L. M. Hocking, *Euro. J. Appl. Math.* **12**, 195 (2001).
  - [15] O. Devauchelle, C. Josserand, and S. Zaleski, *J. Fluid Mech.* **574**, 343 (2007).
  - [16] A. Münch and P. L. Evans, *Physica D* **209**, 164 (2005).